Dyes and Pigments 84 (2010) 237–241

Contents lists available at ScienceDirect

Dyes and Pigments

journal homepage: www.elsevier.com/locate/dyepig

The preparation and characterization of tabular, pearlescent Fe-doped potassium lithium titanate

Xiangwen Liu [a,*], M.K. Devaraju [a], Shu Yin [a], A. Sumiyoshi [b], T. Kumei [b], K. Nishimoto [c], Tsugio Sato [a]

[a] Institute of Multidisciplinary Research for Advanced Materials, Tohoku University, 1-1, Katahira, 2-Chome, Aoba-ku, Sendai 980-8577, Japan
[b] Research institute, Fancl Corporation, 12-13 Kamishinano, Totsuka-Ku, Yohohama 244-0806, Japan
[c] Daito Kasei Kogyo Co., Ltd., 1-6-28, Akagawa, Asahi-ku, Osaka 535-0005, Japan

ARTICLE INFO

Article history:
Received 24 June 2009
Received in revised form
4 September 2009
Accepted 24 September 2009
Available online 6 October 2009

Keywords:
Flux
Tabular
Potassium lithium titanate
Doping
Morphology
Pearlescent
Red shift

ABSTRACT

Potassium chloride was used as flux to prepare tabular crystals of both potassium lithium titanate and Fe-doped potassium lithium titanate employing an optimum mass ratio of flux:raw materials. The effects of the dopant and its concentration and the calcination temperature on the morphology of the Fe-doped potassium lithium titanate were investigated. The crystal phases and optical properties of Fe-doped potassium lithium titanate were characterized using X-ray diffraction analysis and UV–vis spectrophotometry, respectively. The influence of dopant concentration on the colour, band gap narrowing and lattice constants of Fe-doped potassium lithium titanate are discussed.

1. Introduction

Hitherto, layered materials have been widely used as adsorbents, catalysts, catalyst supports and hosts for various functional species, owing to their high chemical stability. Of these compounds, layered transition-metal oxides have been the subject of considerable attention due to their cation exchange [1,2], semiconducting [3,4] and swelling properties [5]. Lepidocrocite titanates ($A_xTi_{2-y}M_yO_4$ where A is an interlayer cation and M, the metal ion or vacancy) are a popular layered transition-metal oxide material owing to their versatile composition [6,7]. Lepidocrocrite titanates, especially potassium lithium titanate (PLT), have been used as starting material for the preparation of various shape-controlled functional materials [8–10]. The synthesis of inorganic materials for application as UV-shielding materials has been reported by the present authors [11–17]. As nanoparticulate inorganic materials generally cannot provide good coverage and are uncomfortable on human skin because of their agglomeration, plate-like particles are often required to enhance their covering ability and comfort. This can be accomplished by the combination of the inorganic nanoparticle with a plate-like titanate such as PLT [18–20]. It is noteworthy that the particle size of the plate-like titanate plays an important role in such functional applications. As colour is also an important consideration for such cosmetic applications, optimization of the preparation conditions for plate-like PLT is required to obtain particles of the desired size, shape and colour.

The aim of this paper was to optimize the reaction conditions used to prepare well-defined, tabular PLT and to synthesize Fe-doped PLT using a flux melting method. To this end, PLT of various colours and sizes was synthesized and the effects of flux quantity on the morphology of PLT and of dopant (Fe^{3+}) concentration on the morphology and colour of Fe-doped PLT were investigated.

2. Experimental

2.1. Synthesis of plate-like potassium lithium titanate-the optimization of flux dosage

The typical procedure to prepare PLT using a flux method was: K_2CO_3, Li_2CO_3 and TiO_2 (anatase form) in the molar ratio of 3:1:13 and an appropriate amount of KCl flux (employing mass ratios of flux:raw materials of 0, 0.09, 0.5, 1.0, 2.1 and 4.0) were ground in an agate mortar. The mixture was placed in a platinum crucible and

* Corresponding author. Fax: +81 06 6872 7485.
E-mail addresses: xwliu@ri.ncvc.go.jp (X. Liu), tsusato@tagen.tohoku.ac.jp (T. Sato).

0143-7208/$ – see front matter © 2009 Elsevier Ltd. All rights reserved.
doi:10.1016/j.dyepig.2009.09.010

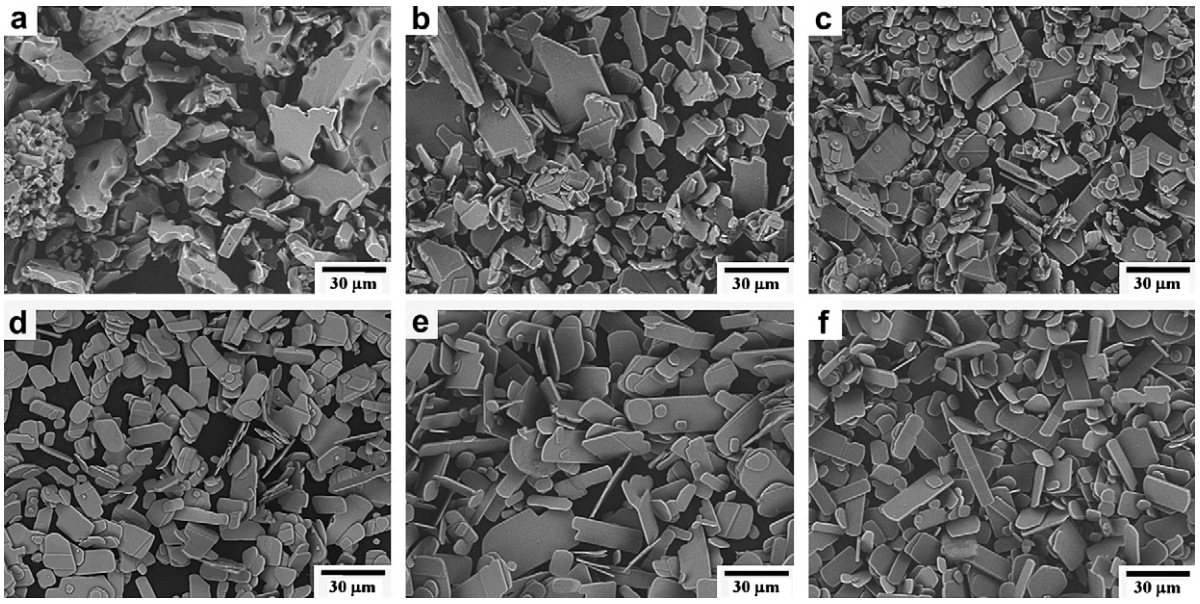

Fig. 1. Typical SEM images of PLT prepared at 1000 °C for 5 h with different mass ratio of flux/raw materials: a) 0.0; b) 0.09; c) 0.5; d) 1.0; e) 2.1; f) 4.

then heated to 1000 °C at a heating rate of 600 °C h^{-1}. The temperature was maintained at 1000 °C for 5 h and the ensiung mixture was allowed to cool to room temperature. Thereafter, the default mass ratio of flux to raw materials was fixed at 1.0. The product was washed with boiling water and filtered to remove the KCl flux and was finally dried at 150 °C for 2 h.

2.2. Synthesis of Fe-doped plate-like potassium lithium titanate

K_2CO_3 (1.355 g), Li_2CO_3 (0.24 g) and TiO_2 (3.405 g) (anatase form) in the molar ratio of 3:1:13 were roughly pre-mixed in an agate mortar. The appropriate iron salt or iron oxide (iron(III) nitrate enneahydrate ($FeNO_3 \cdot 9H_2O$), iron (III) acetylacetonate ($Fe(CH_3COCHCOCH_3)_3$), iron(II) chloride tetrahydrate ($FeCl_2 \cdot 4H_2O$), iron(III) chloride hexahydrate ($FeCl_3 \cdot 6H_2O$), Iron (III) oxide hydroxide (FeOOH), iron oxide (Fe_2O_3) and iron sulfate heptahydate ($FeSO_4 \cdot 7H_2O$)) was added. Then, KCl flux was added and the ensuing intimately ground, placed in a platinum crucible and heated to 1000 °C at a heating rate of 600 °C h^{-1}. The temperature was held at 1000 °C for 5 h and then allowed to cool to room temperature. The product was rinsed with boiling water and filtered to remove the KCl flux and vacuum dried at 150 °C for 2 h. The concentration of iron dopant in PLT was calculated from the molar ratios of Fe/(Fe + PLT).

2.3. Characterization

In order to confirm the crystal phase and investigate the solid solubility limit, X-ray diffraction (XRD) measurement was carried out using graphite monochromatized, CuKα radiation. The lattice parameters of typical samples doped with $FeNO_3 \cdot 9H_2O$ in various concentrations were determined by using pure silicon as an inner standard. The morphologies of samples were evaluated by a field-emission scanning electron microscope (Hitachi, FE-SEM S-4800). The particle size distributions of typical samples were measured by using a laser diffraction particles size analyzer (SHIMADZU, SALD-7000). The catalytic abilities of typical samples for oxidation of organic material were determined by a conductometric determination method (Rancimat method) [18–20] using cosmetic grade castor oil as an oxidized material. UV–vis reflectance spectra were measured using an UV–vis–NIR spectrophotometer (JASCO, V-670).

3. Results and discussion

3.1. The effect of mass ratio of flux/raw material on the morphology of PLT

In order to determine the optimum quantity of KCl flux, PLT was prepared in different mass ratio of flux/raw materials. For the convenience of comparison all the samples were prepared under the same reaction condition, calcination at 1000 °C for 5 h. Typical SEM images of PLT with different mass ratio of flux/raw material are shown in Fig. 1. It is clear that large irregular unshaped particles of PLT were obtained in the absence of KCl flux. Tabular PLT particles with irregular size and morphology could be obtained when the molar ratio is up to 0.09 and or equal to 0.5. When the mass ratio is higher than 0.5, such as 1.0, 2.1 or 4.0, uniform tabular PLT particles

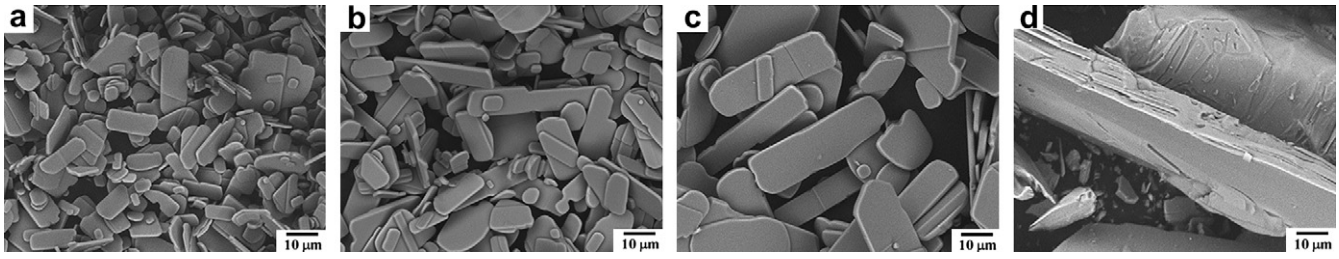

Fig. 2. Typical Images of Fe-doped PLT 6.6% calcinated for 5 h at a) 950 °C; b) 1000 °C; c) 1050 °C; d) 1100 °C.

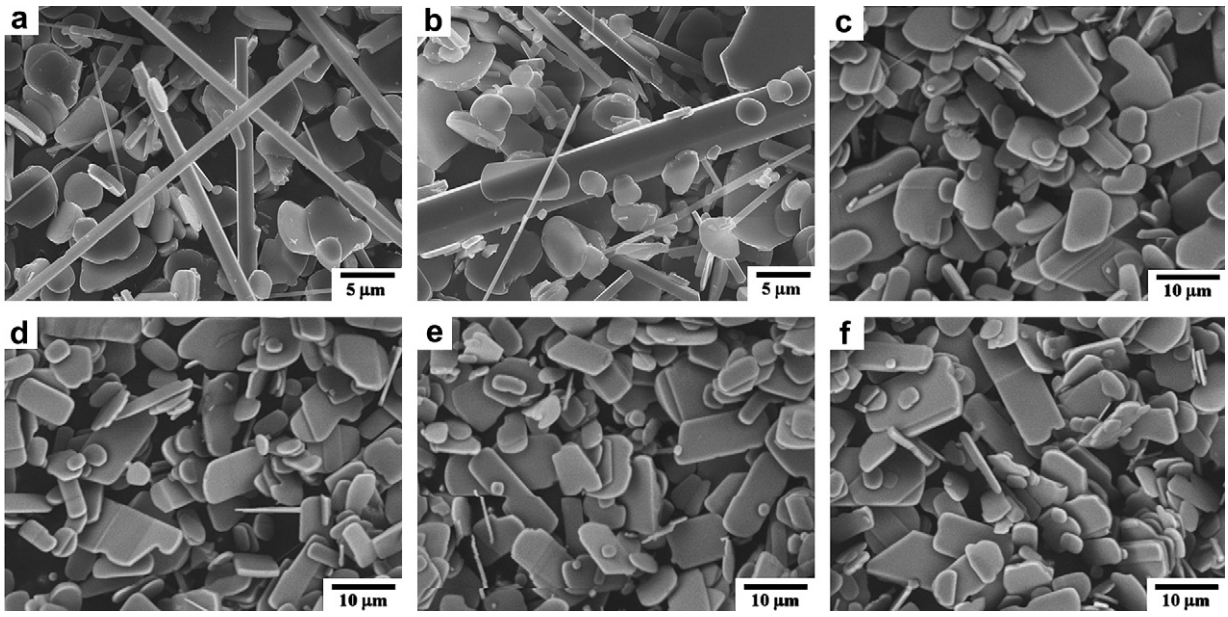

Fig. 3. Typical SEM images of 6.6% Fe-doped PLT particles with different species of iron salts: a) $FeCl_2$; b) $FeCl_3$; c) $Fe(CH_3COCHCOCH_3)_3$; d) $FeSO_4 \cdot 9H_2O$; e) Fe_2O_3; f) FeOOH.

could be obtained. So in order to get well-defined tabular PLT particles the mass ratio of flux/raw materials should not be less than 0.5, and when the mass ratio is higher than 0.5, the further increase has no obvious influence on the morphology change of PLT particles.

3.2. The influence of calcination temperature on the size of Fe doped PLT

In order to investigate the effect of calcination temperature on the morphology and size of sample, parallel experiment was carried out. Typical SEM images of the parallel samples are shown in Fig. 2. It is clear that the average size of sample gradually increased with the enhancement of calcination temperature. However, when the temperature was 1100 °C the size was abruptly increased to more than 100 μm and the morphology was also turned into irregular big particles. So, well-defined tabular sample could be obtained under a calcination temperature below 1100 °C. Hereafter, the 1000 °C was used as the general temperature in the following experiment.

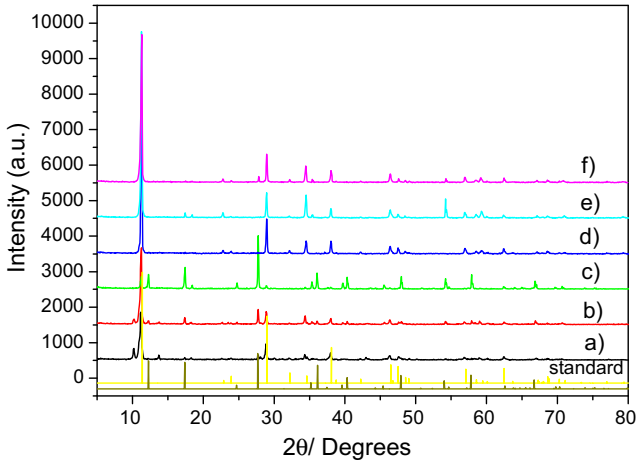

Fig. 4. Typical XRD patterns of 6.6% Fe-doped PLT with different species of iron salts: a) $FeCl_2$; b) $FeCl_3$; c) $Fe(CH_3COCHCOCH_3)_3$; d) $FeSO_4 \cdot 9H_2O$; e) Fe_2O_3; f) FeOOH.

3.3. The effect of doping-salt species on the morphology of PLT (1000 °C, 5 h)

Typical SEM images of PLT particles doped with various species of iron salts with the same doping concentrations of 6.6% are shown in Fig. 3. The images of representative tabular sample, PLT doped with $FeNO_3 \cdot 9H_2O$, will be shown in the following Section 3.4. As we can see that the samples doped with $FeCl_2$ and $FeCl_3$ are multi-morphologies, including tabular sheets, large rod-like sticks and long wires. Both of the samples were repeatedly prepared to confirm the reproducibility and exclude the incidental reason. However, other the samples doped with $Fe(CH_3COCHCOCH_3)_3$, $FeSO_4 \cdot 9H_2O$, Fe_2O_3 and FeOOH respectively are singly tabular sheets with various sizes. The XRD patterns of samples are shown in Fig. 4. Two standard patterns of $K_{1.28}Ti_8O_{16}$ (the first line (olive) from bottom, PDF Card 84–2058) and $K_{0.8}Li_{0.27}Ti_{1.73}O_4$ (the second line (yellow) from bottom, PDF Card 89–5420) are used as the references. Both the tetragonal $K_{1.28}Ti_8O_{16}$ and the orthorhombic $K_{0.8}Li_{0.27}Ti_{1.73}O_4$ are tabular-layered structure. The samples doped with $FeCl_2$, $FeCl_3$, $Fe(CH_3COCHCOCH_3)_3$, and $FeSO_4 \cdot 9H_2O$ are double crystal phases, especially the main crystal phase of $Fe(CH_3COCH\text{-}COCH_3)_3$ doped PLT is $K_{1.28}Ti_8O_{16}$, the main crystal phase of others is $K_{0.8}Li_{0.27}Ti_{1.73}O_4$. The little peaks located around at $2\theta = 10°$ in $FeCl_2$ and $FeCl_3$ doped samples indicated that there should be an inter-layer distance expanding to some extent. The samples doped with Fe_2O_3 and FeOOH are single crystal phase, $K_{0.8}Li_{0.27}Ti_{1.73}O_4$. From all the above mentioned it may be concluded that chloride salts of iron maybe cause the formation of rod-like sticks and wires and the valent difference of iron salts seems no obvious effect on the morphology of PLT particles. Although morphologies of samples doped with $Fe(CH_3COCHCOCH_3)_3$, Fe_2O_3, $FeSO_4 \cdot 9H_2O$ and FeOOH are all singly tabular, doping species of iron have some influence on the crystal phases of according samples.

3.4. The effect of doping concentration on the size, morphology and crystal structure of $FeNO_3 \cdot 9H_2O$ doped PLT

Typical SEM images of PLT doped with various contents of $FeNO_3 \cdot 9H_2O$ are shown in Fig. 5. It is clear that the average size of

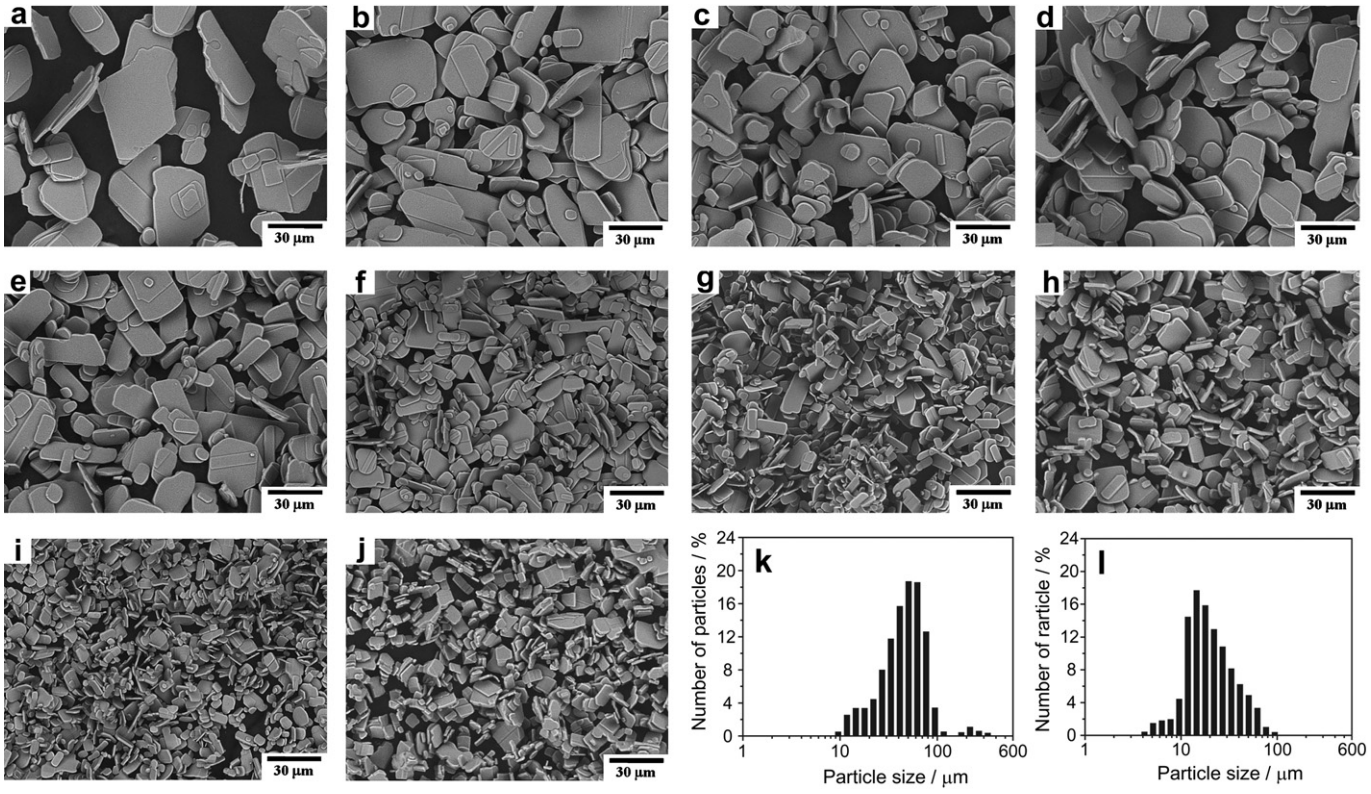

Fig. 5. Typical SEM images of $FeNO_3 \cdot 9H_2O$-doped PLT with different doping concentrations a) 0%; b) 1%; c) 3%; d) 6.6%; e) 11.5%; f) 15%; g) 21%; h) 30%; i) 40%; j) 50% and size distribution patterns of $FeNO_3 \cdot 9H_2O$-doped PLT with concentrations of k) 1% and l) 30%.

samples decreases gradually upon increased doping concentrations of iron. However, when the doping concentration was up to 40% the size increases slightly instead, and sporadic irregular particles was found in the sample. When the doping concentration was up to 50% considerable part of the sample became irregular and big particles. Typical particle size distribution patterns (Fig. 5k,l) shows that the average sizes of $FeNO_3 \cdot 9H_2O$-doped PLT with a doping concentration of 1% and 30% are ca. 50 μm and 12 μm, respectively. As a result, well-defined tabular $FeNO_3 \cdot 9H_2O$-doped PLT particles can be obtained in a wide range of doping concentration.

Typical XRD patterns of $FeNO_3 \cdot 9H_2O$-doped PLT particles are shown in Fig. 6A. All the samples, the doping concentration from 0% to 50%, show a good single crystal phase as pure PLT, not any impure peaks are found in them. That means all the iron ions were doped into the crystal lattice. Although the shape of partial particles of $FeNO_3 \cdot 9H_2O$-doped PLT with doping concentrations of 40% and 50% became irregular, no peaks of impurities were found in XRD patterns. That means higher doping concentration has no obvious influence on the crystal phase but on the morphology. According to the curves of the lattice constants relative to doping concentrations shown in Fig. 6B, it seems that even the 50% doping concentration has not yet reached the solubility limit of iron in PLT, which should be attributed to the mild ionic radii difference between six-coordinated Fe^{3+} (0.645 Å) and Ti^{4+} (0.605 Å) [21]. This also should be the reason for the increase of lattice constants of $FeNO_3 \cdot 9H_2O$-doped PLT upon the increased doping concentrations. In other words, the interlayer space was gradually enlarged due to the larger ionic radium of the Fe^{3+} than that of equally six-coordinated Ti^{4+}. Accordingly, with the increase of doping concentrations a slight shift of the strongest peaks (020) to lower 2θ can also be found (Fig. 6A).

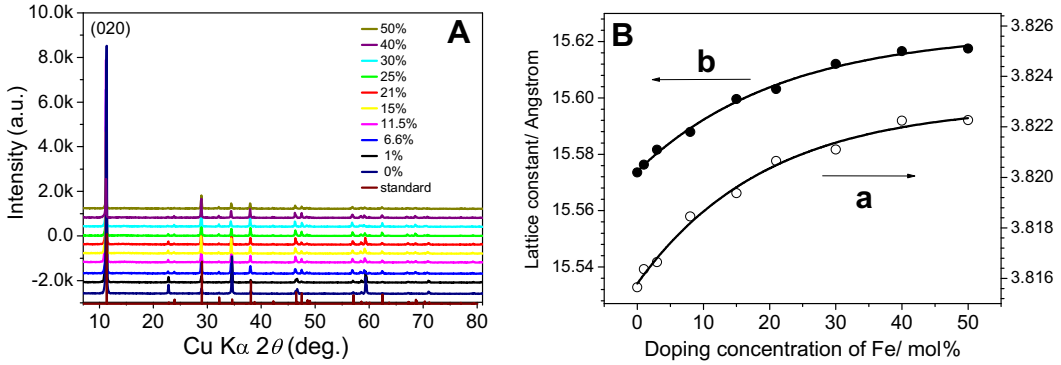

Fig. 6. A) Typical XRD patterns and B) curves of lattice constants versus doping concentration of $FeNO_3 \cdot 9H_2O$-doped PLT.

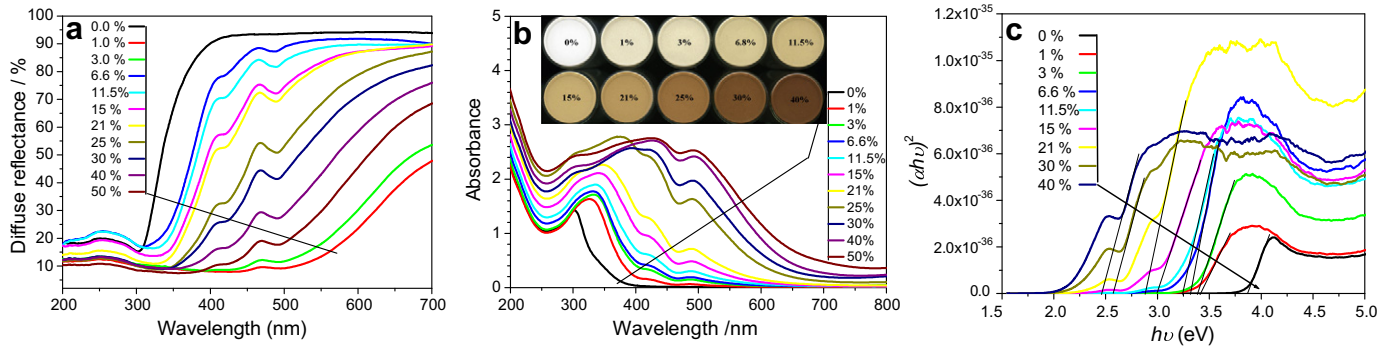

Fig. 7. a) diffraction reflectance spectra; b) Schuster-Kubelka-Munk absorbance plot and c) variation of $(\alpha h\upsilon)^2$ with $h\upsilon$ of $FeNO_3 \cdot 9H_2O$-doped PLT with various concentrations. The inset of b) is the digital scanning photos of PLT and Fe-doped PLT with various doping concentrations.

3.5. The effect of doping concentration on the colour and band gap of $FeNO_3 \cdot 9H_2O$-doped PLT

The UV–vis diffuse reflectance spectra of typical samples are shown in Fig. 7a. The absorption spectra obtained from the diffuse reflectance spectra using Kubelka-Munk analysis and digital scanning photo of $FeNO_3 \cdot 9H_2O$-doped PLT with various doping concentrations are shown in Fig. 7b. It is clear that the absorption shifts from the UV to the visible region with increasing dopant concentrations. The colour of the samples gradually changes from white to red, which is accompanied by a reduction in lightness. In addition, the intensity of pearlescent luster gradually decays owing to the corresponding reduction in average size, which is consistent with the SEM results obtained. Unfortunately, due to limit of the scanning quality the pearlescent luster of the sample is not clear.

Generally, in order to shift the band gap transition to the visible spectral region so as to utilize solar energy more efficiently, metal ion doping is a promising methods used for semiconductors [22]. The metal ion dopant alters the intrinsic electronic structure and acts as electron or hole trap which increases the photoinduced electron/hole charge recombination lifetimes, which, in turn, enhance photocatalytic activity. Owing to its particular electronic structure and its similar ionic radii size to that of titanium (IV), doping with iron (III) has been widely investigated [23,24]. The optical band gap *Eg* can be determined by the following equation for a semiconductor: $(\alpha h\upsilon)^n = B\,(h\upsilon - Eg)$, where $h\upsilon$ is the photo energy, α is the absorption constant, B is a constant relative to the material, and n is either 2 for a direct band gap or 1/2 for an indirect band gap. The $(\alpha h\upsilon)^2 \sim h\upsilon$ curves of various $FeNO_3 \cdot 9H_2O$-doped PLT are shown in Fig. 7c. The band gap of pure PLT is about 3.82 eV. The spectra show a red shift in the band gap transition with increased doping concentrations. The red shift should be attributed to the charge-transfer transitions between the metal ion *d* electrons and the PLT conduction or valence band [25,26], and the band gap narrowing caused by the heavy-doping effect [27].

Table 1
CIE $L^*a^*b^*$ values and Eg of as-prepared pigments.

Fe content	L^*	a^*	b^*	Eg (eV)
Fe 0%	96.08	−1.03	2.74	3.82
Fe 1%	91.45	0.22	9.75	3.43
Fe 3%	87.37	1.79	14.23	3.38
Fe 6.6%	85.70	2.79	15.48	3.32
Fe 11.5%	82.48	4.80	18.03	3.24
Fe 15%	78.44	7.40	21.09	3.00
Fe 21%	74.38	9.40	22.53	2.88
Fe 25%	62.82	14.76	22.46	/
Fe 30%	58.33	14.56	18.68	2.58
Fe 40%	51.39	11.78	11.91	2.46

The CIE $L^*a^*b^*$ (under illuminant D_{65}) and Eg values of $FeNO_3 \cdot 9H_2O$-doped PLT in various doping concentrations are listed out in Table 1, according to which, an increase in dopant concentration reduces lightness and the colour becomes redder.

4. Conclusions

Calcination temperature and dopant concentration influence the size of both PLT and Fe-doped PLT. Owing to the similar ionic radii of Fe^{3+} and Ti^{4+}, it was possible to dope PLT with Fe over a wide range of concentrations ranging from 1% to 50% to secure red, tabular, pearlescent, Fe-doped PLT.

Acknowledgements

This research was partially supported by the Ministry of Education, Culture, Sports, Science and Technology, Scientific Research of Priority Areas "Panoscopic Assembling and High Ordered Functions for Rare Earth Materials" and "Special Education and Research Expenses, Post-Silicon Materials and Devices Research Alliance".

References

[1] Lagaly G, Beneke K. Colloid Polym Sci 1991;269:1198–211.
[2] Raveau B. Rev Chim Miner 1984;21:391–400.
[3] Kim YI, Salim S, Huq MJ, Mallouk TE. J Am Chem Soc 1991;113:9561–3.
[4] Shibata M, Kudo A, Tanaka A, Domen K, Maruya K, Onishi T. Chem Lett 1987;6:1017–8.
[5] Keller SW, Kim HN, Mallouk TE. J Am Chem Soc 1994;116:8817–8.
[6] Reid AF, Mumme WG, Wadsley AD. Acta Crystallogr Sect B 1968;24:1228–33.
[7] Groult D, Mercey C, Raveau BJ. Solid State Chem 1980;32:289–96.
[8] Tanaka T, Ebina Y, Takada K, Kurashima K, Sasaki T. Chem Mater 2003;15:3564–8.
[9] Sasaki T, Nakano S, Yamauchi S, Watanabe M. Chem Mater 1997;9:602–8.
[10] Feng Q, Hirasawa M, Yanagisawa K. Chem Mater 2001;13:290–6.
[11] Yabe S, Yamashita M, Momose S, Tahira K, Yoshida S, Li R, et al. Int J Inorg Mater 2001;3:1003–8.
[12] Yabe S, Sato TJ. Solid State Chem 2003;171:7–11.
[13] Yabe S, Yamashita M, Momose S, Yoshida S, Hasegawa K, Yin S, et al. Inorg Mater Jpn 2001;8:428–33.
[14] El-Toni AM, Yin S, Hayasakab Y, Sato TJ. Mater Chem 2005;15:1293–7.
[15] Li R, Yabe S, Yamashita M, Momose S, Yoshida S, Yin S, et al. Solid State Ionics 2002;151:235–41.
[16] Li R, Yabe S, Yamashita M, Momose S, Yoshida S, Yin S, et al. Mater Chem Phys 2002;75:39–44.
[17] El-Toni A, Yin S, Sato T. Mater Chem Phys 2007;103:345–50.
[18] Liu XW, Yin S, Sato T. Mater Chem Phys 2009;116:421–5.
[19] Liu XW, Yin S, Sato T. Mater Sci Eng 2009;1. 012013.
[20] Liu XW, Liu JX, Dong XL, Yin S, Sato TJ. Colloid Interface Sci 2009;336:150–4.
[21] James GS. Lange's handbook of chemistry. 16th ed. CD&W inc.; 2005. p. 1153.
[22] Choi W, Termin A, Hoffmann MR. J Phys Chem B 1994;98:13669–79.
[23] Litter MI, Navio JA. J Photochem Photobiol A 1996;98:171–81.
[24] Ranjit KT, Viswanathan B. J Photochem Photobiol A 1997;108:79–84.
[25] Moser J, Gratzel M, Gallay R. Helv Chim Acta 1987;70:1596–604.
[26] Borgarello E, Kiwi J, Gratzel M, Pelizzetti E, Visca MJ. Am Chem Socs 1982;104:2996–8.
[27] Antonio L, Steven H, editors. Handbook of photovoltaic science and engineering. Chichester: John Wiley & Sons; 2003. p. 70.